J. Biomechanics Vol. 12, pp. 657–678.

0021-9290/79/0901-0657 $02.00/0

VISCOELASTIC PROPERTIES OF WET CORTICAL BONE—I. TORSIONAL AND BIAXIAL STUDIES*†

RODERIC S. LAKES

U. Wisconsin

and

J. LAWRENCE KATZ‡ and SANFORD S. STERNSTEIN§

Center for Biomedical Engineering‡ and Materials Engineering Department,§
Rensselaer Polytechnic Institute, Troy, NY 12181, U.S.A.

Abstract – The dynamic moduli for frequencies between 2×10^{-3} and 100 Hz and the relaxation modulus between 1 and 10^5 sec have been measured in torsion for human and bovine cortical bone kept wet in Ringer's solution, as a function of temperature, strain-level and a superposed axial load. At body temperature, the dynamic loss tangent increased from 0.009 at 100 Hz, to 0.013 at 1 Hz, to 0.025 below 0.1 Hz. The total change in shear modulus over 8 decades of time-scale was 15–35%, most of this change occurring at long times in relaxation. Bovine bone, although stiffer, exhibited viscoelastic behavior similar to that of human bone.

Nonlinear viscoelastic response, in the form of the isochronous shear modulus increasing with strain level, became apparent for strains above 10^{-4}, and was observed to be less pronounced in dynamic tests than in relaxation. Recovery at long times occurred more slowly than relaxation, but always approached completion asymptotically. This effect, small in human bone and negligible in bovine bone, is accentuated by the superposition of an axial stress on the torsion sample.

Biaxial experiments were performed, since bones in the body are subjected to stresses which are more complex than uniaxial tension or shear. An axial tensile stress of 17.2 MN/m^2 increased the high frequency loss tangent of human bone by $\simeq 20\%$ and changed the shear modulus by $\simeq 1.5\%$; for bovine bone, the shear modulus was changed by 0.6% by an axial stress of 22.1 MN/m^2.

The temperature dependence of the viscoelastic response was found to be thermorheologically complex. This implies that bone experiments must be done at body temperature to be relevant to the *in vivo* situation, and that time–temperature superposition is of questionable validity for bone.

INTRODUCTION

Interest in the behavior of bone as a structural element in the human body has motivated a large number of investigations into the mechanical properties of bone; for extensive and comprehensive reviews, the interested reader is referred to the reviews by Evans (1973) and Katz and Mow (1973).

Examination of the response of bone to stress began well over 100 years ago, when Wertheim (1847) determined the breaking strength of human bone in tension for female fibula and femur, and for male fibula and femur. A considerably more detailed investigation undertaken by Rauber (1876) included measurements of breaking strength in tension and compression, the modulus of elasticity in bending, both for wet and dry bone, as well as anisotropy, and even study demonstrating viscoelastic response (creep); dry bone was shown to be both stiffer and stronger than wet bone. Over 80 years later, Smith and Walmsley (1959) made the following observations on wet human tibial bone: (i) the modulus of elasticity (Young's modulus) in compression exceeds that in tension by about 3%; (ii) bone creeps in tension by $\sim 16\%$ of the 'initial' elongation in 20 min and recovery seems to be asymptotic to zero; (iii) bone contracts with water loss; (iv) in bending, the compliance of bone increases linearly with temperature by about 15% in the range 50–110°F, and the effect of temperature on elasticity is reversible; (v) the Young's modulus measured in tension exceeds that in cantilever bending by a factor between 1 and 1.7. Anisotropy in compression of human cortical bone was examined by Dempster and Liddicoat (1959). Bones were found to be stiffer in compression than in tension for wet bones, but the reverse was true (to a lesser extent) for dry bones. These data, as well as measurements of breaking strengths, were compared with corresponding values for common woods, stones and metal. The stiffness of bone exceeds that of most woods, and its strength exceeds that of most woods and stones, as well as brick and concrete. Young's modulus tests were done at a stress rate of 200 psi/min; 'wet' samples were obtained by soaking previously dry material for 24 hr. More detailed investigations of the anisotropy of bone were performed using ultrasonic techniques by Lang (1969) on bovine cortical bone, and by Yoon and Katz (1976a, b) on human cortical bone. Both experimenters reported that their results were consistent with a hexagonal 'texture' symmetry. In the latter case, the following elements of the elastic modulus tensor C_{ijkl} for dry human compact bone at ultrasonic frequencies were obtained‡: $C_{1111} = 23.4$, $C_{3333} = 32.5$, $C_{2323} = 8.71$, $C_{1122} = 9.06$, $C_{1133} = 9.11$,

* *Received* 22 *August* 1977.

† This paper is based on part of a dissertation submitted by R. S. Lakes, while an N.I.H. Predoctoral Trainee, in partial fulfillment of the requirements for the Ph.D. in Physics at Rensselaer Polytechnic Institute.

‡ The 3-axis here is parallel to the bone axis.

$C_{1212} = 7.17$, in units of GN/m^2 (where 1 GN/m^2 $\cong$ 1.45×10^5 psi). This is consistent with the finding of Dempster and Liddicoat that the compressional Young's moduli in the two transverse directions are equivalent, but contradicts Bird *et al.* (1968) and Lugassy and Korostoff (1969), who assert that they are not. The larger specimens used in these experiments may account for this, since cortical bone exhibits a gradient in porosity in the radial direction (Smith and Walmsley, 1959).

Studies of viscoelastic properties of bone which attempt to go further than simply demonstrating the existence of such effects have not been done until comparatively recently. Smith and Keiper (1965), for example, examined the dynamic response of wet bones from different parts of the human body, over the frequency range 500–3500 Hz at a strain of 10^{-4}. The storage modulus in compression/tension was found to average 15.9 GN/m^2 and the loss tangent (obtained from the measured loss modulus) averaged 0.025 for 4 femoral bone samples. The storage modulus was independent of frequency within the resolution of their equipment. Currey (1965) examined the long-term creep behavior of wet bovine tibial and metacarpal bone in cantilever bending and made the following observations: (i) creep, measured in the range 2 min–10 days and plotted vs log time, gives a curve which is always concave up (room temperature); (ii) recovery following this test appeared to be asymptotic toward zero strain after 100 days; (iii) in repeating the creep experiment, the maximum difference in the deflections was only 5% initially and almost nothing later. After 55 days, the creep curve was still concave up through the entire time range; (iv) dry bone exhibited less creep than wet, but irreversible effects due to drying were not marked; (v) creep deflection at a given time was proportional to load; (vi) creep deflection after 2 min and 2 hr depends on temperature in the range 2.5–48°C; (vii) at body temperature, recovery following 1 day of creep is asymptotic to zero strain; in the range 2 min–54 days, the creep curve (deflection vs log time) is always concave upward. Deflection at the end of 54 days is 2.36 times the 'initial' deflection. Attack by bacteria and fungi was prevented by a crystal of thymol dissolved in the water bath. In contrast to this very long time behavior, experiments by Bird *et al.* (1968) disclosed the following dependence of the compressional stiffness on stress rate: at a stress-rate of 1.38 MN/m^2 sec, $E = 21.4$ GN/m^2; at a stress rate of 1.72 GN/m^2 sec, $E = 26.2$ GN/m^2. These values are for the longitudinal direction; similar experiments were done for the radial and tangential directions. McElhaney (1966) measured the compressional stiffness of wet femoral compact bone for six strain-rates over a wide range. Results for fresh bovine bone followed a similar pattern; however, the energy absorbed to fracture as a function of strain-rate was different. Stress–relaxation data taken by Lugassy and Korostoff (1969) for wet bovine femoral cortical bone in compression, in different directions, were originally fitted to straight lines in a relaxation modulus vs log-time plot.

Dynamic experiments by Black and Korostoff (1973) showed the storage modulus of viable, wet, human tibial compact bone to increase from 6.35–10.0 GN/m^2 at 35.4 Hz up to 12.1–14.9 GN/m^2 at 353.6 Hz. Although resolution was limited, anomalous sudden changes in the dynamic modulus near 200 Hz were reported.

A number of experiments have been done on very small pieces of bone in an effort to elucidate the relationships between the structure and physical properties of bone. Bonfield and Li (1967), for example, examined the torsional properties of filaments, 254 μm dia., of bovine tibial compact bone. They found: (i) 'nonelastic' effects for stresses greater than 3.9 MN/m^2; recovery was not made; (ii) the shear modulus was 5.6–6.1 GN/m^2; (iii) anisotropy in hysteresis and nonelastic effects. Ascenzi and Bonucci (1966) were able to isolate segments of human single osteons and obtain values of Young's modulus in compression for fully calcified osteons. Values for osteons which were least calcified were found to be lower than for fully calcified. Frasca (1974) also examined the dynamic torsional response of human single osteons using a new technique which was developed to isolate osteons long enough for this purpose.

THE BOLTZMANN SUPERPOSITION INTEGRAL

If a material is subjected to a step-function strain history (in one dimension), $\varepsilon(t) = \varepsilon_0 H(t)$, where $H(t)$ is the unit step function and t is time, the resulting stress history can be written $\sigma(t) = G(t).\ \varepsilon_0$, where $G(t)$ is a function characteristic of the material and is called the relaxation modulus. Boltzmann's Superposition Principle states that the effect of a compound cause is the linear superposition of the effects of the individual causes. When a 'box function', $\varepsilon(t) = \varepsilon_0[H(t-t_1) - H(t-t_2)]$, is considered to be the compound cause,† then the resulting stress history must be

$$\sigma(t) = [G(t-t_1) - G(t-t_2)]\varepsilon_0, \quad \text{for } t > t_2 > t_1. \tag{1}$$

Now, consider an arbitrary strain history $\varepsilon(\tau)$ which is zero before time $\tau = 0$; then the stress at the present time t due to an element of strain history between time τ and $\tau + d\tau$ can be expressed as

$$\begin{aligned} d\sigma(t) &= [G(t-\tau-d\tau) - G(t-\tau)]\varepsilon(\tau) \\ &= -\frac{dG(t-\tau)}{d\tau}\varepsilon(\tau)d\tau. \end{aligned} \tag{2}$$

The total stress now at time t is the limit of the sum (integral) of all such expressions, as $d\tau$ becomes arbitrarily small, i.e.

† This corresponds to a relaxation and recovery experiment.

$$\sigma(t) = -\int_0^t \frac{dG(t-\tau)}{d\tau}\varepsilon(\tau)d\tau + \varepsilon(t)G(0), \quad (3)$$

where the second term is the stress due to the strain at the present time, which does not relax. Integrating this by parts yields the Boltzmann Superposition integral in its usual form, a constitutive equation for a linearly viscoelastic material

$$\sigma(t) = \int_0^t G(t-\tau)\frac{d\varepsilon(\tau)}{d\tau}d\tau \quad (4)$$

$$\sigma_{ij}(t) = \int_0^t C_{ijkl}(t-\tau) \times \frac{d\varepsilon_{kl}(\tau)}{d\tau}d\tau \text{ (three-dimensional form).} \quad (5)$$

This last expression is the simplest one capable of adequately describing the viscoelastic behavior of bone. Its significance lies in the fact that, once the kernel function C_{ijkl} (or G in one dimension for shear) is known, the stress response to *any* strain history, however complex, can be calculated. The kernel can be obtained by experiments employing *simple* strain histories (e.g. sine wave, step function). In addition, linearly viscoelastic materials are characterized by stiffness parameters which depend on time (or frequency), but not on strain level. This simplicity of behavior is not found in materials which are non-linearly viscoelastic.

Although the experiments described earlier clearly showed the existence of viscoelastic behavior in bone, the linearity of the response has generally been assumed rather than demonstrated. In an effort to compare the results of various experiments done on bone, the resulting viscoelastic functions were transformed into a common representation (Lakes and Katz, 1974) using the theory of linear viscoelasticity described above. The lack of agreement among the results, as well as the failure of results of individual experiments to satisfy internal consistency tests, led to the conclusion that cortical bone in compression appears to be non-linearly viscoelastic. Therefore, the present study was undertaken to examine the torsional and biaxial viscoelastic behavior of cortical bone. The results are published in this series of three papers:

Part I deals with the experimental techniques and the data obtained on human and bovine wet compact bone;

Part II develops a set of hypothetical relaxation mechanisms which are treated theoretically in an attempt to understand some of the causes of viscoelasticity in wet compact bone;

Part III deals with the non-linear viscoelastic behavior and develops a constitutive equation for wet compact bone.

EXPERIMENTAL EQUIPMENT AND METHODS

The instrument used in the viscoelastic measurements described below is a biaxial, driven torsion pendulum designed and constructed in the laboratory of one of us (S.S.S.) for the characterization of glassy polymers. The mechanical portion of this instrument has been described previously by Paterno (1970) and was used in conjunction with dynamic viscoelastic studies on rubber modified thermoplastics such as high impact polystyrene. Subsequently, the electronic components of the instrument have been redesigned and a closed loop servo system incorporated, thereby enabling creep and stress relaxation studies to be performed on the torsion pendulum. The programmable closed loop servo is the same as used on a tension/compression viscoelastic tester, which has been used for mechanical aging studies on glassy polymers (Myers *et al.*, 1976) and which will be described elsewhere (Myers and Sternstein, 1977). The latter system is currently being used to study the viscoelastic properties of bone in tension and compression and will be reported on at a later date (Haelen and Sternstein, 1977).

A simplified schematic of the mechanical portion of the biaxial driven torsion pendulum is shown in Fig. 1. The instrument is programmable under closed loop

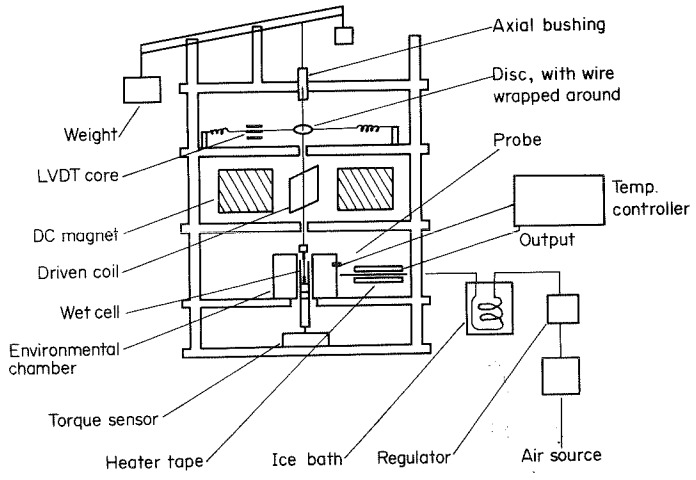

Fig. 1. Schematic of the biaxial torsion pendulum.

control of either torque or angular displacement insofar as the torsional mode of sample deformation is concerned, but can be used to apply only static loads (or zero load) in the axial deformation mode of the sample. Thus, torsional creep, torsional stress relaxation and torsional dynamic mechanical spectra can be obtained with or without the superimposition of a fixed axial stress.

With reference to Fig. 1, the frame of the torsional pendulum is exceedingly robust and massive, with the major support posts consisting of threaded 1 in. dia. steel rods and major (stress or torque reacting) support plates constructed of 1 in. thick steel plates. The mechanical assembly weighs about 300 lb and is supported by a 'sand bath' which greatly minimizes building vibrations being transmitted to the sample. The torsion motor is basically a stalled rotor motor when connected to the sample and produces torque and angular displacements which are sufficient to deform a steel sample 2 in. long and $\frac{1}{8}$ in. dia. to *ca.* 0.1% strain.

The motor consists of a d.c. magnet assembly and a lightweight, low inertia magnesium rotor frame containing many turns of fine wire (the driven coil). The rotor frame is rigidly connected to upper and lower connecting shafts which are supported by rotary bearings containing press fitted linear bearings. Thus, the entire rotor assembly is free to both rotate and move axially between the magnet pole pieces, which are long enough to allow substantial axial motion within the magnetic field. The rotary motion or torque is determined by the signal applied to the driven coil, whereas the axial motion is associated only with the axial creep of the sample under an applied axial load, as described below. In effect, the driven coil transmits any axial load applied to it directly to the sample load.

The upper rotor connecting shaft is connected to a fine elastic wire, the other end of which is connected to an axial bushing (a dovetail slide), which can move axially, but does not rotate. The axial bushing is connected to a lever arm which is counterbalanced to support the weight of the entire rotor assembly. In biaxial experiments, a weight is applied to the lever arm, which is then reacted by a force transmitted via the axial bushing to the suspension wire, to the rotor assembly and then to the sample. The torque developed by the rotor is superposed on the axial force. In pure torsion experiments, the counterbalanced lever results in no axial force on the sample.

The upper rotor connecting shaft also supports a small disc containing a circumferential groove. A fine wire is wrapped around this disc and connected at both ends with springs to the instrument frame. An LVDT core is mounted concentrically to and along the wire. The housing of the LVDT is mounted to the frame with provisions for axial alignment and zeroing. This system is used to convert the angular displacement of the rotor into a proportional linear motion. Mechanical gain of the motion is also provided by the disc diameter which was nominally 1 in. The torsional stiffness of the rotor assembly and torque sensor (see below) is *ca.* 18,000 in.–oz/radian, which exceeds the stiffness of the samples used by several decades. Thus, little error is introduced by measuring the angular displacement at the position shown in Fig. 1. The two mounting springs for the fine wire supporting the LVDT core are carefully balanced to give zero torque when the sample is not being tested.

The lower rotor connecting shaft is connected to a sample grip which clamps the sample. The other end of the sample is connected to a second sample grip which is connected to a reaction torque sensor (Lebow Associates, 100 in.–oz capacity) which utilizes a strain gage bridge. A bakelite connector is used between the lower grip and torque sensor in order to minimize heat conduction from the sample to the sensor and surroundings.

The torque sensor and LVDT signals were processed using two carrier amplifiers whose carrier waves were phase locked to eliminate beat frequency effects during dynamic measurements. Calibration of the LVDT was accomplished with a micrometer screw. The linear range of the LVDT is ± 0.050 in., which in conjunction with the 1 in. dia. disc, allowed the full scale sensitivity of the carrier amplifier to be set as high as ± 5 mrad (angular displacement) per ± 10 V output. Lower sensitivities were also used for 'high strain' experiments, the limit being ± 40 mrad/± 10 V output, due to the restricted linear range of the LVDT.

Primary calibration of the torque sensor was accomplished using precision weights, fine wires and a torque bar of known lever arm. Secondary calibration was accomplished using a shunt resistor across one arm of the torque sensor bridge and the results of the primary calibration. Full scale sensitivities ranging from ± 10 to ± 100 in.oz/± 10 V output are easily obtained.

Since the resolution of the output voltages from both carrier amplifiers exceeded one part in one thousand, angular displacements of 0.005 mrad and torques of 0.01 in. oz could be detected. The initial system consisted of Daytronic Model 300 carrier amplifiers, which displayed noise in their outputs of 10–20 mV P-P from 1 to 5 Hz, and 100 mV near 0.01 Hz, in addition to carrier feedthrough of 50 mV at 3 KHz. In addition, these amplifiers gave zero drift of *ca.* 1% per day and sensitivity drift of 1.5% per day, both at the most sensitive range used. The amplifiers were replaced prior to experiment No. 7 by Daytronic Model 800 carrier amplifiers, whose noise outputs were lower by as much as a factor of ten. Sensitivity drift was also reduced to 0.1% per day, but zero drift remained about 1%.

The noise and drift of the carrier amplifiers proved to be the limiting factor in resolution and performance of the torsion pendulum. Errors due to friction or closed loop servo drift were, in general, lower than the errors associated with the transducer carrier amplifiers.

Stress relaxation experiments were performed under closed loop control, using the angular displacement

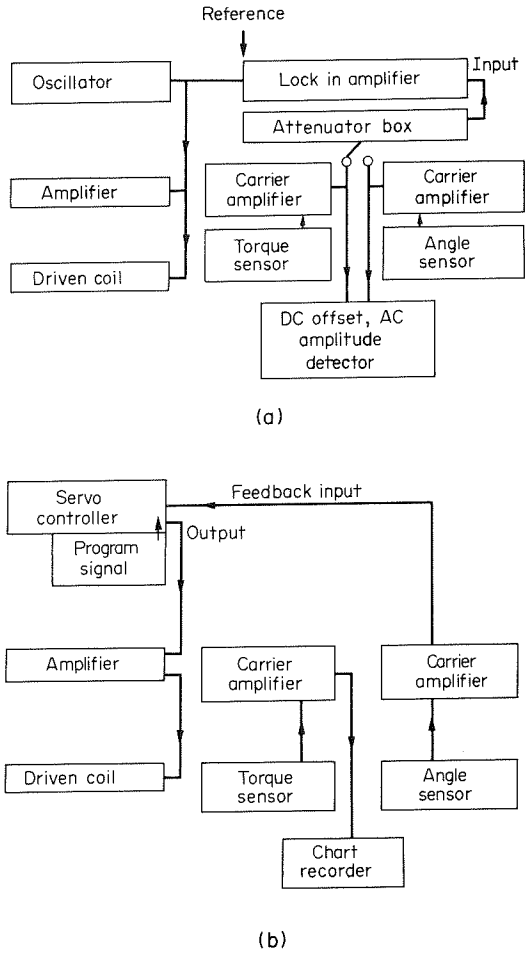

Fig. 2. Schematic of the electronics for the viscoelastic experiments. (a) = dynamic experiment, (b) = stress relaxation.

signal as feedback. A simplified schematic is shown in Fig. 2. The servo controller is of original design and utilizes PID (proportional, integral and derivative) control. The various break points associated with the gain vs frequency response of the servo are all adjustable, thereby enabling a wide range of response functions and apparatuses to be controlled. In the case of the torsion pendulum described above, the servo cutoff frequency was limited to 50 Hz, thereby ensuring absolute stability of the servo system–torsion pendulum combination. The risetime of a step function angular displacement (for a stress relaxation test) was electronically controlled to 60–100 msec for zero to final value of angle. This ensured the absence of ringing, instability and overshoot.

Since a specimen with fading memory behavior cannot distinguish between a perfectly sharp step function strain history and a 'rounded' history after a time greater than ten risetimes,† relaxation data for the present instrument were considered valid at times equal to or greater than 1 sec. (The same servo system, when used with the tension–compression apparatus, can load a sample in 10–20 msec without overshoot.)

The control stability of the servo system, i.e. the maximum change in the controlled variable (angle, in this case) is about 1 part in 10,000. Thus, insofar as the closed loop system is concerned, the limiting factor on the constancy of the strain during a stress relaxation test is the degree to which a constant output voltage from the angle carrier amplifier corresponds to a constant angle. Clearly, sensitivity drift or zero drift of the transducer and its amplifier become the limiting factors in maintaining constant angle. The system utilizing the Daytronic carrier amplifiers, Model 800, was sufficiently 'stiff' (drift free) to allow accurate stress relaxation tests to be performed at shear strains as low as 10^{-5}.

Dynamic (sinusoidal) experiments were performed using the torsion pendulum open loop, but driven (not free decay) at constant amplitude for each frequency. The open loop mode allowed operation to 100 Hz. With reference to Fig. 2, an oscillator signal of the

† Ferry (1970) shows this for a linear solid by deriving the stress response to a program of constant strain rate followed by constant strain, and comparing this with the stress resulting from a true step function strain; see also Turner (1973).

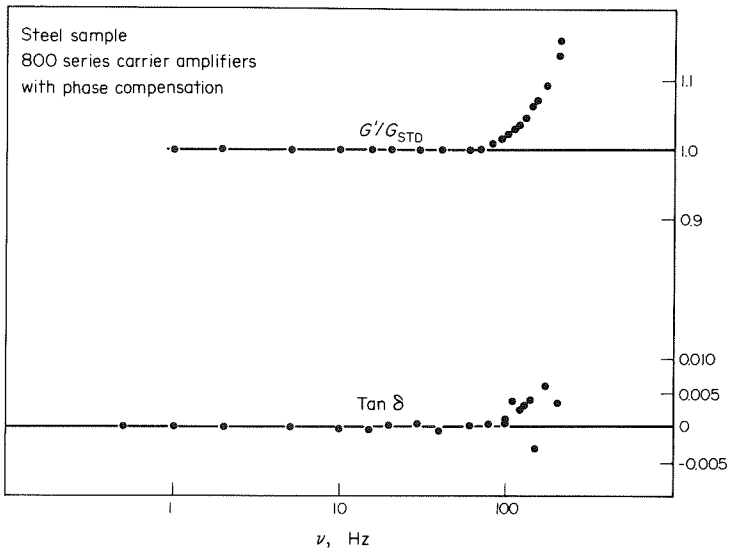

Fig. 3. Measured response of a steel specimen as a control.

desired frequency was fed directly to the power amplifier which fed the driven coil. The torque and angle signals were attenuated and fed into a two phase lock-in amplifier (Princeton Applied Research, Model 129A). The attenuation was chosen such that a 10 V peak–center sine wave would give a full scale reading on the 100 mV (rms) scale of the lock-in. The reference signal for the lock-in was a pure square wave output from the oscillator which was frequency and phase coherent with the sine wave output. This ensured a jitter free, sharply defined zero crossing point for the lock-in reference, which was especially useful at low frequencies.

Since phase shifts invariably occur in any a.c. motor, a differential measurement of phase angle was required. First, the angle signal was used as the signal input to the lock-in and the reference phase shift adjusted for zero quadrature signal. Then the torque signal was used as an input signal and its phase measured with respect to the angle null, thereby eliminating motor phase shift.

In order to ensure that the sine wave was symmetric with respect to zero torque, a dual peak detector was used to determine the d.c. component of the torque signal. The instrument enabled a d.c. component of less than 1 part in 1000 of the a.c. component to be detected. If a d.c. component was present, it was removed by applying a d.c. bias to the power amplifier. Thus, all dynamic measurements were performed on samples which were free of torsional creep.

The calibration procedures described previously were d.c. calibrations of torque and angle which do not calibrate for potential phase shift and gain change at higher frequencies. To accomplish an a.c. calibration, measurements were made on a steel sample at room temperature. Such a sample is essentially elastic. The in-phase shear modulus G' and loss factor $\tan\delta$ obtained with the lock-in amplifier are shown vs frequency in Fig. 3. Clearly, the gain and phase shift of the transducers and carrier amplifiers are flat to 100 Hz. Above this frequency, the erratic results are due to a resonance in the angle transducer mechanical assembly. (A small phase lag was required in one of the carrier amplifiers to obtain the flat response below 100 Hz.)

The dynamic experiments are not significantly affected by amplifier noise and drift, since the lock-in amplifier detects only signals at the same frequency as the reference signal. Since for bone the quadrature component of the torque signal is only about 1% of the component in phase with the angle signal, the measurement of the former requires considerable sensitivity. For this system, the resolution of $\tan\delta$ (i.e. quadrature torque divided by torque in phase with angular displacement) was better than 0.0005, for pure sine wave signals. Noise in the actual signals degraded this to about 0.001 or better. The usable frequency range for dynamic experiments was limited from below at 0.5 Hz by the lock-in amplifier and from above at 100 Hz by resonances in the LVDT.

The properties of bone, as well as polymers, depend upon both temperature and moisture content, therefore it is necessary that both be held constant during the experiments. In order to approximate most closely to conditions within the body, bone specimens were kept immersed in Ringer's solution prior to, and during, the experiments. The wet chamber illustrated in Fig. 4 was designed to accomplish this. Temperature control is achieved using a Dynapac model 15 proportional temperature controller in the configuration shown in Fig. 1. Air passes from a laboratory wall nozzle into an environmental specimen chamber after passing through a heat exchanger, followed by a copper pipe wrapped with electrical heater tape, whose energy is supplied by the temperature controller. For experiments near or below room temperature, the heat

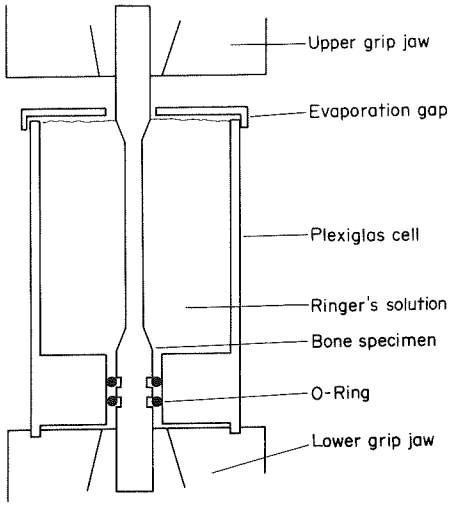

Fig. 4. Schematic of the wet cell for the bone specimens.

exchanger tank is filled with ice and water; for experiments at temperatures above room temperature, the tank is empty. Prior to the experiments with specimen 7, the system was modified as follows: the air was preheated by passing it through a heater box powered by a variable transformer. This reduced the output required of the temperature controller and so improved the temperature stability of the system.

In winter, the dryness of the air leads to more rapid evaporation of water from the wet cell. Therefore, the air was bubbled through a heated flask of water before being passed through the preheater box. In order to prevent damage in the event that the backpressure from the water shut off the air flow, thus opening the temperature-control feedback loop, a thermal cutout device was built. This device, consisting of a bimetallic thermal relay, mounted above the heater tape, and a relay, shuts off the heater power if the heater tape gets too hot.

The specimen chamber itself consists of an aluminum labyrinth through which the air passes, insulated by 1 in. of styrofoam. Inserted into the labyrinth are the probe for the temperature controller and one junction of a copper–constantan thermocouple used to monitor the temperature. The other junction is inserted in a dewar flask containing distilled water and ice prepared from distilled water at 0°C. Escape of the air between the grip jaws and the labyrinth bore is reduced by a baffle plate mounted above the upper grip.

Since relaxation kinetics depend on temperature, variations in specimen temperature introduce error in the measured relaxation modulus or dynamic modulus. In torsion, the effect of temperature variations is not nearly as serious as in tension or compression, since while a homogeneous solid will expand with an increase in temperature, it will not twist. Inhomogeneities in several bovine bone specimens caused a small thermal torsion effect. The estimated error in the relaxation modulus due to this is less than 0.5%; specific specimens are discussed under experimental results. Temperature variation over long times was generally less than 0.2°C; temperature oscillation (for certain runs, discussed later) was less than 0.2°C. Error in the relaxation and dynamic moduli, estimated from the dependence of these moduli on temperature, is 0.2%.

Friction in the pendulum bearings can be static or kinetic. Kinetic friction, if small, is unlikely to adversely affect either the dynamic or transient response of the system. Static friction or 'stiction' can introduce undesirable hysteresis, which can cause instability in the closed-loop, servo controlled configuration. Moreover, in a dynamic experiment, a sinusoidal driving signal will not produce a sinusoidal angular displacement if static friction is present. Static friction, as determined by 'tweaking' the pendulum with a specimen in place and observing the residual angular displacement, is less than 5×10^{-4} of the angular displacement used in the 'large' strain experiments (25 mrad). Static friction levels less than half the above figure could usually be obtained by alignment of the pendulum and LVDT. Errors due to friction, beyond those attributable to noise, could not be detected.

To reduce the friction initially present, both pendulum bearings were removed, soaked and cleaned in kerosene, and lubricated with light sewing machine oil. After remounting, the bearings were realigned.

In summary, then, the ranges of frequency, strain and time over which viscoelastic measurements can be made accurately are limited by the torsion pendulum and the associated electronics. These limits for the experiments described herein are as shown in Table 1.

SAMPLE PREPARATION

Samples of both human and bovine bone were taken from the midshaft of long bones. The ends were first sawn off and the resulting piece cut lengthwise into

Table 1. Limits of frequency, strain and time used in the experiments

Frequency	2×10^{-3} Hz $\leq \nu \leq$ 100 Hz
Dynamic strain	$10^{-6} \leq \gamma \leq 10^{-3}$
Relaxation strain	$10^{-5} \leq \gamma \leq 2 \times 10^{-3}$
Time	1 sec $\leq t \leq (1-5) \times 10^5$ sec

The lower limit in frequency was set by the *experimenter's patience*.

quarters using a bandsaw. During this cutting the bones were never more than slightly warm to the touch. The pieces were then turned down on a lathe into the cylindrical shape shown in longitudinal section in Fig. 4. Cutting was done slowly under a drip of Ringer's solution so that the sample was permitted neither to dry out nor to become perceptibly warm. Final sample dimensions were: grip end diameter, 0.313 and 0.310 in. for upper and lower grips, respectively, gauge diameter 0.125 in., gauge length 1.25 in., overall length 3.37 in. Adapters were also made for those bone samples not thick enough to obtain the above dimensions. The sample, held in place by stainless-steel setscrews, had the following dimensions: gauge length 1 in., gauge diameter 0.120 in., grip end diameter 0.188 in., overall length 2.313 in. Small variations from the above dimensions were permitted.

To prevent the decay of the sample by bacterial or fungal attack during lengthy experiments, a dilute solution of bactericide and antibiotics, described in Appendix 1, was added to the Ringer's solution bath.

After storage of a few days or less, under refrigeration (unless stated otherwise), a bone sample was placed in the instrument and the jaws tightened. Since the upper grip end of the sample was exposed to the air, it partially dried and consequently shrank; the upper jaw had to be retightened after one day. Changes in the properties of the thick gripped end were of no consequence, since its compliance (inversely proportional to the fourth power of the radius) was much smaller than that of the gauge section. Samples mounted with adapters were immersed throughout in the Ringer's solution.

With the sample in place, the environmental chamber was mounted and the lower shaft fixed to the torque sensor by tightening setscrews in such a way that the torque-motor was properly centered. The carrier amplifiers were nulled and the sensitivity adjusted for proper calibration. Since the zeroing of the torque amplifier was done when the torque sensor was free of any torque (sample not connected to it), the re-zeroing after mounting was done by tensioning the LVDT springs so that the actual torque was zero. Coarse zeroing of the LVDT was done by translating the barrel, and fine zeroing by adjustment of the amplifier.

† In a fading-memory material, the effect due to a strain history of finite duration approaches zero asymptotically as time approaches infinity.

At this point, the pendulum was 'tweaked' to see if it would return to the same position. If the frictional response exceeded the values given above, the LVDT core was moved laterally a small amount. This was necessary since precise lateral alignment of the core could not be done visually, due to the presence of the LVDT cage. If the friction could not be adequately reduced by repeating this procedure, the lower shaft was disconnected from the torque sensor, moved a small amount, and reconnected. This was repeated until the friction was minimized.

After a few hours, the chamber temperature, which was monitored on a chart recorder, reached the value dictated by the temperature controller, and the experiments were begun in the following order. First, the dynamic experiments were performed at a number of strain levels, the average value of the torque signal as determined by the peak-reader being adjusted to zero by the offset control on the Kepco amplifier. Then the servo-controller was connected, as shown in Fig. 2, with the feedback signal coming from the torque amplifier so that the torque could be controlled at zero and the angular displacement followed on the chart recorder. When the angle had reached a constant value, the angle amplifier was zeroed and the feedback was taken from it so the angle could be controlled at zero and the torque signal monitored. If the torque deviated slightly from zero, it was reset using the zero adjustment on the *angle* amplifier (which was providing the feedback signal) so that zero torque signal still corresponded to zero torque. Now the strain-level was set on the servo-controller, the chart recorder turned on and a stress–relaxation experiment at small strain-level begun by applying a step-function program signal to the servo-controller. The recovery was then observed by reversing the leads to the recorder and setting the program voltage to zero. When the torque-signal in recovery became sufficiently small, a large-strain stress experiment, followed by recovery, was done. The small-strain experiment was done first so that error due to residual recovery stress remaining after a finite time was minimized. If experiments were to be done at more than one temperature, the shaft was disconnected from the torque sensor, the temperature control setting raised (thus accelerating any residual recovery) and the above procedure repeated.

While it might be objected that the above procedure is justified only if bone is a fading-memory material,† the alternative procedure of using a fresh sample for each experiment is unacceptable, since individual bones and pieces of bone differ sufficiently in their structural properties that a set of exactly identical samples cannot be obtained. However, the repeatability of the experiments, as described later, tends to support the fading-memory hypothesis for bone, at the strain levels used.

Several changes in the procedure were made when the 800-series carrier amplifiers and data logger became available. Adequate resolution was obtained using the 300-series carrier amplifiers by means of a

zero-suppression feature consisting of an adjustable d.c. voltage subtracted from the signal voltage permitting the use of a more sensitive amplifier scale. Suppression voltage was set using the chart recorder, since the control dial was not accurately calibrated. This was unnecessary with the 800-series amplifiers, since the digital data logger used with them printed the signal voltages to 4 figures. Sufficient suppression to observe accurately the relaxation for times less than 1 min was obtained using the zero offset control on the recorder. Adjustable low-pass active filters included with the 800-series amplifiers permitted not only the reduction of noise in the relaxation curve, but also extension of the low-frequency range in dynamic experiments. Use of the 100 Hz filters eliminated the 3 kHz carrier noise, yet introduced negligible phase-shifts below 1 Hz, yielding torque and angle signals sufficiently clean to be displayed on an oscilloscope as a Lissajous figure. The relation between the observed width of the elliptical figure and the loss tangent is given in Appendix 2. Although the figure was observed for at least ten cycles even at the lowest frequencies used, no visible change in the loss tangent was seen after the first cycle.

Since various changes were made in the experimental set-up and procedure in an effort to improve resolution and reduce errors, a summary of experimental details is given below.

Specimens 1, 2, *bovine femur*

These results are not presented here since control of temperature, experimental resolution and preparation techniques were significantly improved in later experiments.

Specimen 3, *bovine femur*

An oil layer above the Ringer's solution was used to reduce evaporation in long-term experiments. This oil was not permitted to contact or absorb into the gauge section of the specimen. At this point, the use of the zero offset knob and output expansion on the lock-in amplifier, rather than reading the meter directly, was begun. This significantly improved resolution in the storage modulus measurement. For this experiment and subsequent ones, the use of the readings on the carrier amplifier suppression dial were abandoned, due to inaccuracies in its calibration. Actual suppression voltage was measured using the chart recorder.

Specimen 4, *human tibia*

These results were rejected as artifactual, since oil was permitted to contact the gauge sections of this specimen.

Specimens 5, 6, *human tibia*

The air-dryer used for polymer experiments was bypassed by altering the plumbing; no oil was used in these and subsequent experiments. Water evaporation in this and previous experiments was compensated for by adding distilled water at the sample temperature. Since this had to be done every 12–24 hr, the long-term relaxation experiments were perturbed thermally by the removal of half the chamber to add the water. Since this could be done quickly, the thermal perturbation was small and lasted less than 20 min. It was arranged that the water replacement was done at long times in relaxation or recovery so that the perturbation had sufficient time to be 'forgotten' between data points; these specimens required adapters.

Specimen 7, *bovine femur*

The 300-series carrier amplifiers were now replaced by the 800-series amplifiers and data logger. The air was now bubbled through warmed water before going to the specimen chamber. The chamber was drilled with a small hole so that a tubule ((1/32 in., clear rubber) could be passed outside in order that the water could be replenished using a syringe, without opening the chamber. A steel sample was subjected to dynamic testing, prior to this bone experiment, both for calibration at higher frequencies and to verify the absence of phase-shifts below 1 Hz in the Lissajous figure mode, with both 100 Hz filters in.

Specimen 8, *bovine tibia*

Relaxation and dynamic experiments were done at a large number of strain levels using the procedure employed for specimen 7. Following recovery from the 'large strain', i.e. 6.2×10^{-4} relaxation experiment, a strain 4 times larger was applied for 100 sec and the sample allowed to recover for several days. Following this recovery, the relaxation experiment at a strain level of 6.2×10^{-4} was repeated under identical conditions in order to test for the effects of prolonged immersion on the mechanical properties.

Specimen 9, *bovine femur*

The procedure was identical to that for specimen 7 for the relaxation and dynamic experiments. Following these experiments, the generation of harmonics at relatively large amplitude dynamic strains was examined by driving the sample at a given frequency and supplying the reference input to the lock-in amplifier with a sinusoidal signal at a multiple of that frequency. Since oscillators that could be phase-locked were not obtainable for this, only the magnitude of the harmonic signal was measured.

Of the nine original specimens tested, the results on six, 2 human and 4 bovine, are presented in this article.

RESULTS AND DISCUSSION

The results of the viscoelastic experiments are presented in Figs. 5–20. Although the response of each bone specimen is unique, the curves share a number of common features. First, the dynamic loss tangent is of the order 0.01 in the domain 0.5–100 Hz and generally has a larger value at the lower frequencies. For those experiments in which the domain below 0.5 Hz was examined, $\tan \delta$ increased to about 0.025 below 0.1 Hz. Second, most of the change in shear modulus occurred at long times in relaxation. Third, nonlinear response in the form of an increase of the shear modulus with strain-level is seen in relaxation and, to a lesser extent, in those dynamic experiments done at larger strains.

Although there are many similarities in the mechanical properties of human and bovine bone, there can be considerable differences in the microstructural level of organization. This can be seen in Fig. 21, where a transverse section of normal adult human femoral cortical bone is compared with a similar section from a young bovine femur. These structural differences (Haversian vs plexiform) must be considered in any serious attempt to theoretically predict the properties of bone.

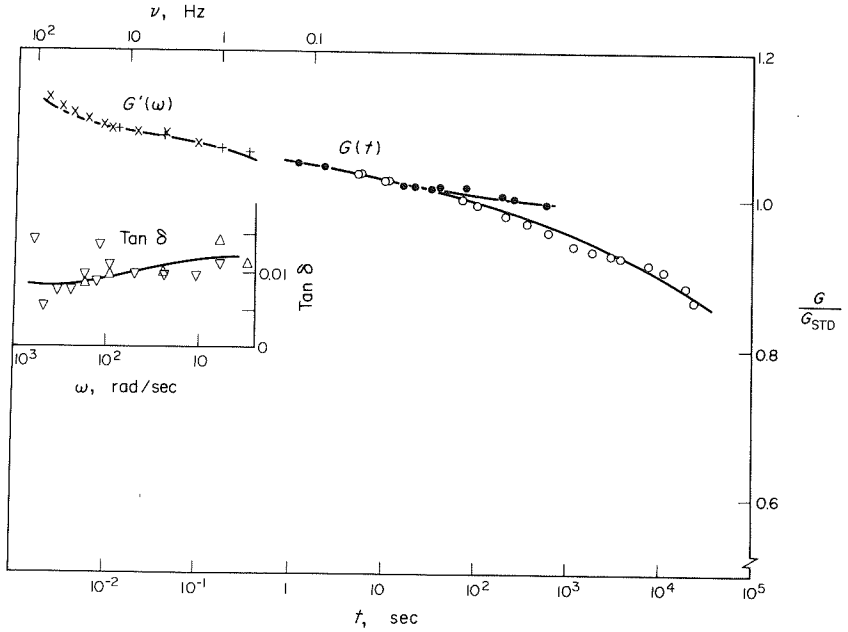

Fig. 5. Viscoelastic response in wet bovine femoral bone, specimen 3; $T = 28°C$.

○ Relaxation $\gamma = 5.5 \times 10^{-4}$
● Relaxation $\gamma = 5.5 \times 10^{-5}$
+ △ Dynamic $\gamma = 2.2 \times 10^{-5}$
× ▽ Dynamic $\gamma = 2.2 \times 10^{-4}$

Simple torsion

$G_{STD} = G(t)|^{37°C}_{10\,sec} = 7.75 \times 10^5 lb/in^2$.

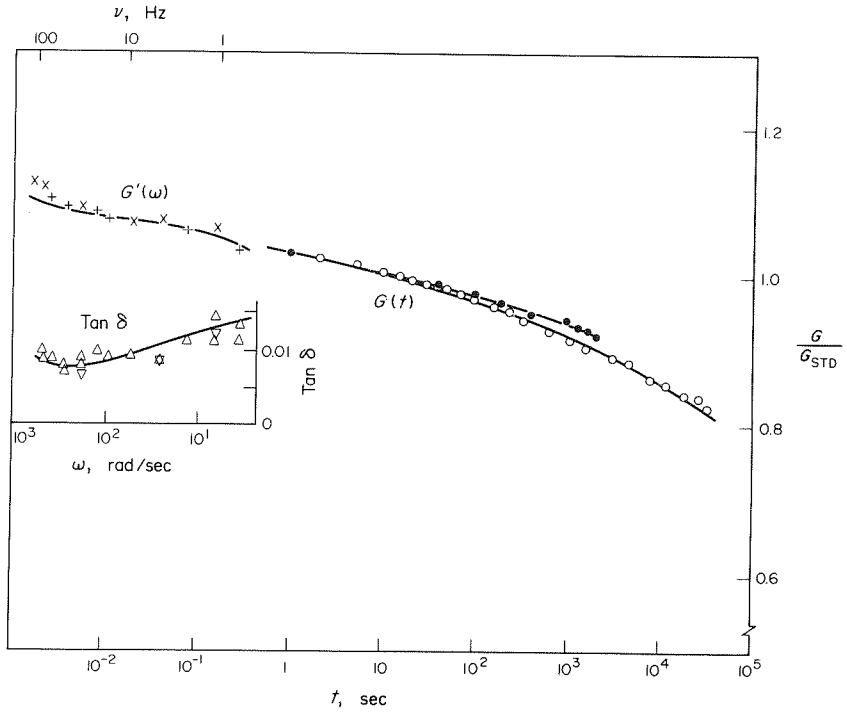

Fig. 6. Viscoelastic response in wet bovine femoral bone, specimen 3; $T = 37°C$. Torsion values and symbols as for Fig. 5.

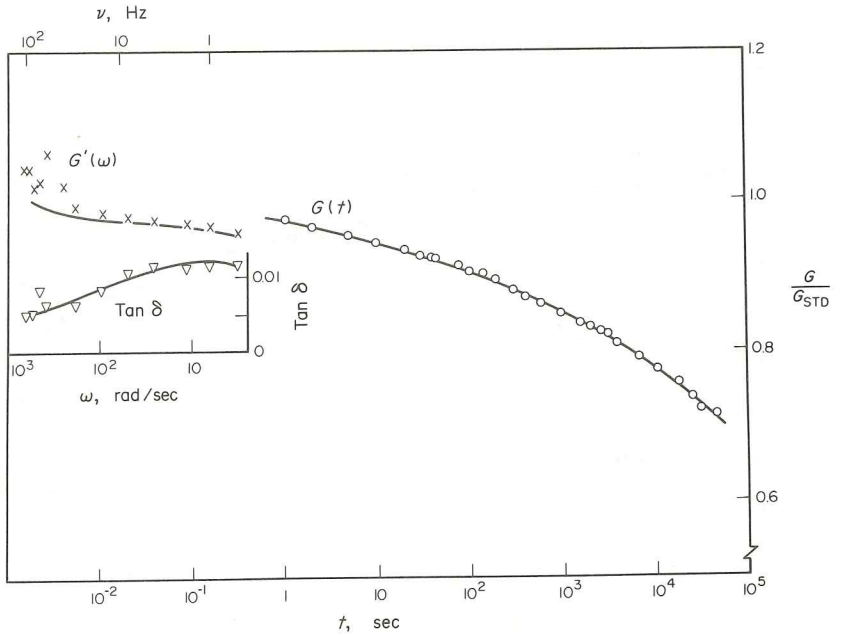

Fig. 7. Viscoelastic response in wet bovine femoral bone, specimen 3; $T = 47°C$. Torsion values and symbols as for Fig. 5.

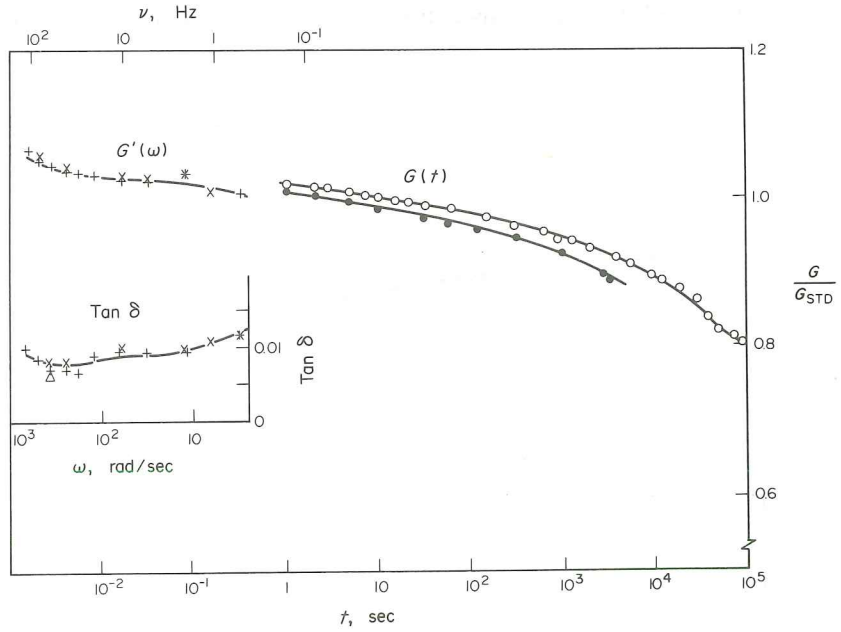

Fig. 8. Viscoelastic response in human tibial bone, specimen 6; $T = 37°C$.

○ Relaxation $\gamma = 9 \times 10^{-4}$
● Relaxation $\gamma = 9 \times 10^{-5}$
△ Dynamic $\gamma = 3.6 \times 10^{-6}$
\+ Dynamic $\gamma = 3.6 \times 10^{-5}$
× Dynamic $\gamma = 3.6 \times 10^{-4}$

Simple torsion

$G_{STD} = 0.602 \times 10^6 \text{lb/in}^2$
$= G(10\,\text{sec}, 37°C)$.

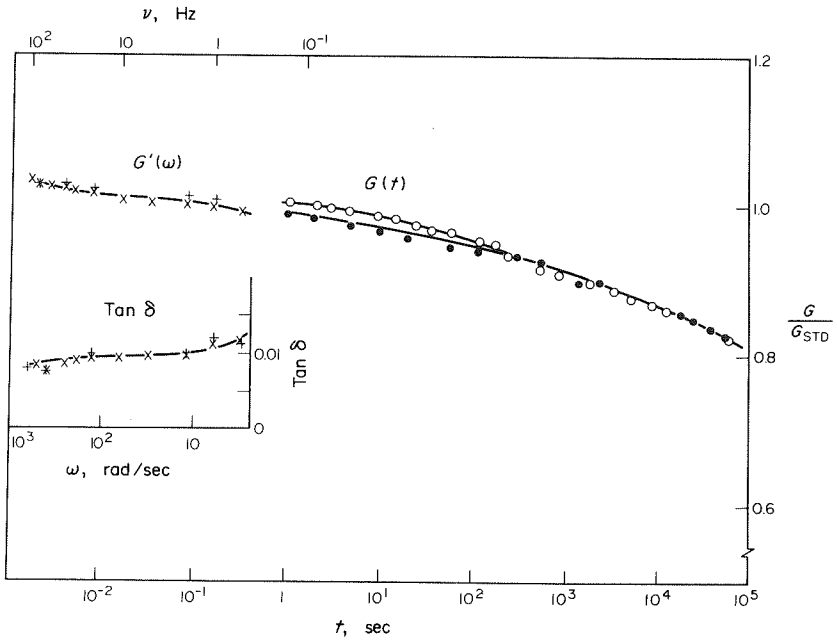

Fig. 9. Viscoelastic response in human tibial bone, specimen 6; $T = 41.6°C$. Torsion values and symbols as for Fig. 8.

It is impossible to prepare a set of truly identical specimens of bone. Therefore, it was necessary to subject the individual specimens to prolonged periods of immersion in Ringer's solution during the course of successive experiments. This led to concern about the possible introduction of artifacts due to the prolonged immersion. The tests done on specimen 8 provide an assessment of the magnitude of such artifacts. A one-day stress–relaxation experiment was performed ($\varepsilon = 6.2 \times 10^{-4}$) followed by sufficient time at zero strain

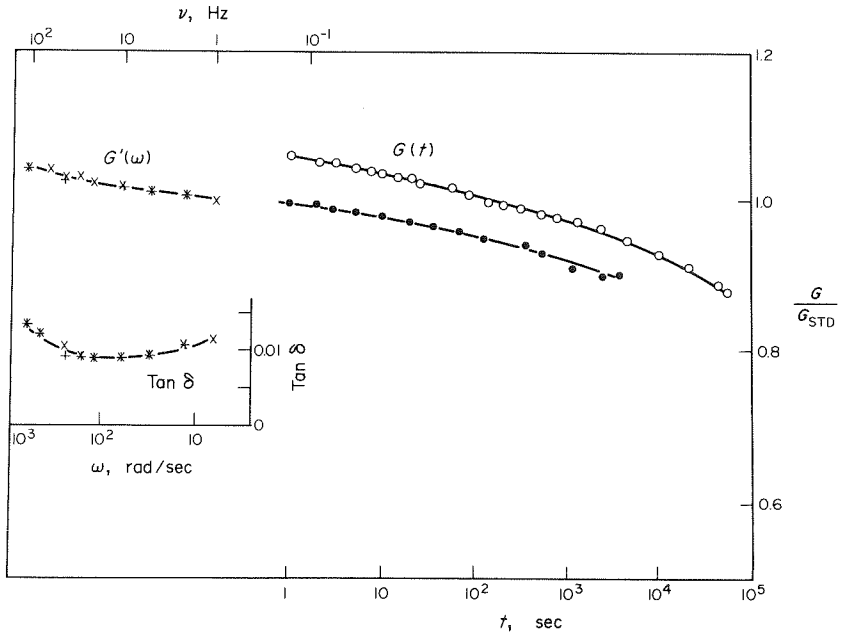

Fig. 10. Viscoelastic response in bovine femoral bone, specimen 7; $T = 28.4°C$.

● Relaxation $\gamma = 1.21 \times 10^{-4}$
○ Relaxation $\gamma = 6.19 \times 10^{-4}$
\+ Dynamic $\gamma = 2.32 \times 10^{-5}$
× Dynamic $\gamma = 2.32 \times 10^{-4}$

$G_{STD} = 8.37 \times 10^5 \text{lb/in}^2$.

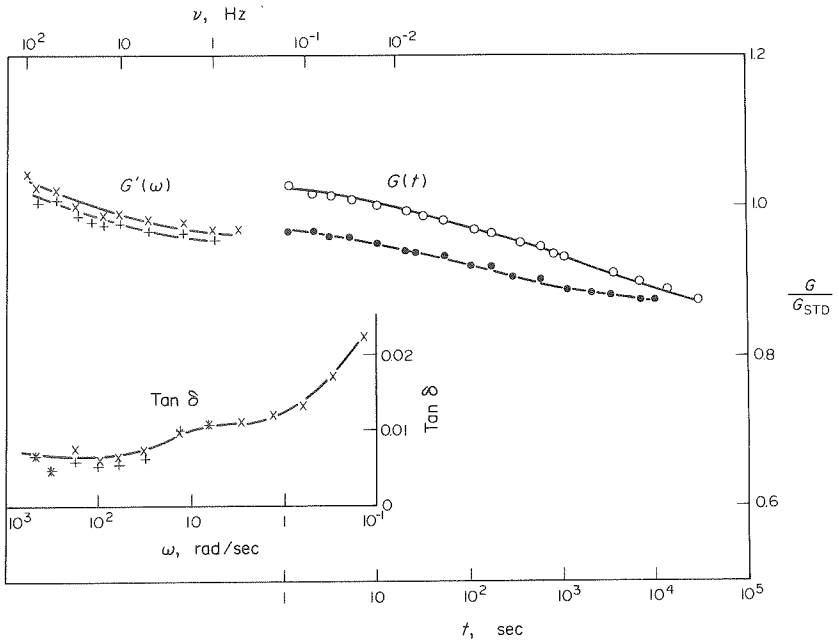

Fig. 11. Viscoelastic response in bovine femoral bone, specimen 7; $T = 37°C$.

● Relaxation $\gamma = 1.18 \times 10^{-4}$
○ Relaxation $\gamma = 6.15 \times 10^{-4}$
\+ Dynamic $\gamma = 2.32 \times 10^{-5}$
× Dynamic $\gamma = 2.32 \times 10^{-4}$

$G_{STD} = 8.37 \times 10^5 \text{lb/in}^2$.

(about one week) to allow for essentially complete recovery. A second one-day relaxation experiment, performed subsequently under identical conditions, yielded results virtually identical to the results of the first experiment, as shown by the data points labeled by circles and squares, respectively, in Fig. 13. The procedure of soaking bone specimens in Ringer's solution was therefore judged to have an insignificant effect on their mechanical properties.

It is also conceivable that strains as small as

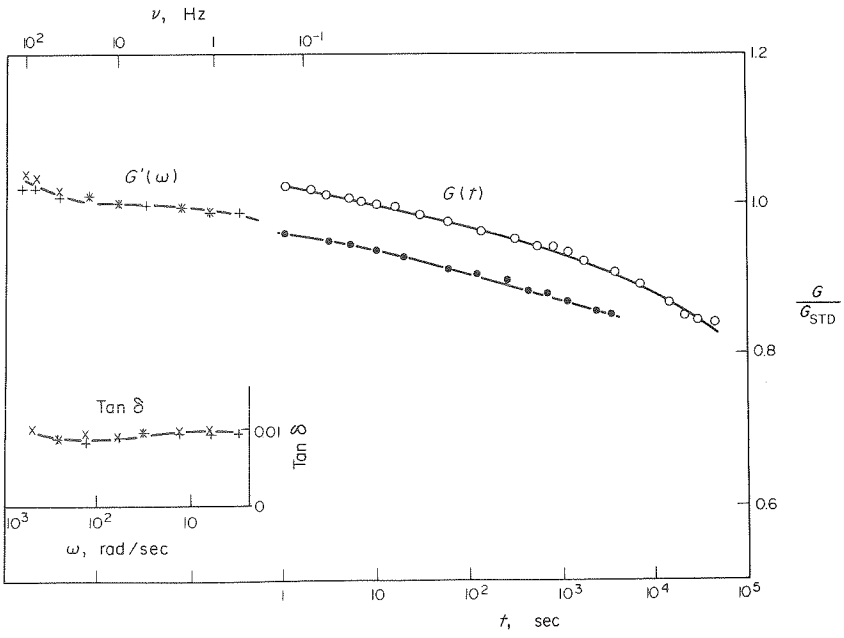

Fig. 12. Viscoelastic response in bovine femoral bone, specimen 7; $T = 43°C$. Torsion values and symbols as for Fig. 11.

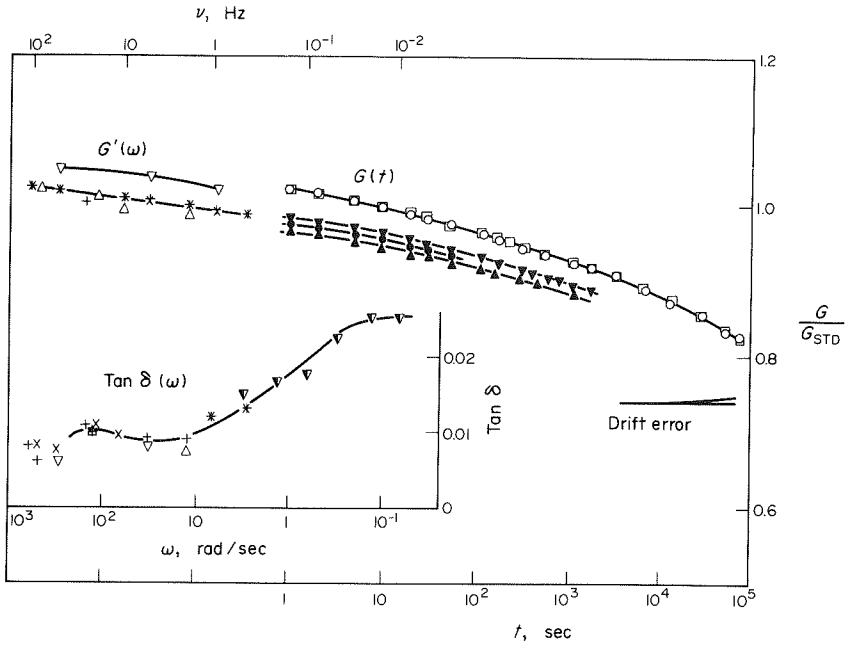

Fig. 13. Viscoelastic response in bovine tibial bone, specimen 8; $T = 36.7°C$.

● Relaxation $\gamma = 4.66 \times 10^{-5}$
▲ Relaxation $\gamma = 6.61 \times 10^{-5}$
▼ Relaxation $\gamma = 3.09 \times 10^{-4}$
○, □ Relaxation $\gamma = 6.19 \times 10^{-4}$
△ Dynamic $\gamma = 1.61 \times 10^{-6}$
+ Dynamic $\gamma = 1.61 \times 10^{-5}$
× Dynamic $\gamma = 1.61 \times 10^{-4}$
▽ Dynamic $\gamma = 6.24 \times 10^{-4}$
▼ Dynamic $\gamma = 4.16 \times 10^{-4}$
$G_{STD} = 8.34 \times 10^{5}$ lb/in².

6.2×10^{-4} might lead to irreversible changes in the bone specimens. The above results suggest that this does not occur. To explore this issue further, specimen 8 was subjected to a strain pulse of duration 120 sec and amplitude 2.5×10^{-3} prior to the second-day experiment described above. The excellent agreement between the data represented by squares and circles in Fig. 13 suggests that strains considerably larger than those used in the other experiments have no permanent effect on the specimens.

Specimens 3, 6 and 7 were studied at more than one temperature. For certain types of materials, it is found that a graph of a viscoelastic response function vs long time or log frequency can be superimposed on a similar graph obtained at a different temperature, by a shift along the abscissa (Ferry, 1970). Such materials are called thermorheologically simple. None of the graphs obtained for bone in the present work, however, can be superposed in this way (Figs. 5–12). This observation is significant in the interpretation of previous experiments with bone. Some such previously published results were obtained at temperatures other than body temperature, or else the temperature was not quoted. The thermorheological complexity of bone precludes the simple extraction of the response at body temperature from such results. Thermal complexity is also suggestive of multiple response mechanisms but does not specify what they may be.

As stated above, nonlinear behavior is observed in the torsion of compact bone. This takes the form of an increase in the shear modulus at short and intermediate times with strain level, and accelerated long-term relaxation at higher strains. This shear stiffening is not seen for strains below $1.6–3.6 \times 10^{-4}$ in dynamic experiments (except for specimen 7).

However, in relaxation experiments done at many strain levels (specimen 8, Fig. 13), this effect is resolvable above estimated errors for a strain of 7×10^{-5}. At equal peak strains, dynamic shear stiffening is less than relaxational shear stiffening (specimen 9, Fig. 14). This pattern of nonlinear behavior is consistent with the two types of constitutive equations discussed in Part III.

Comparisons between the relaxation and recovery moduli $G(t)$ and $R(t)$ are plotted in Figs. 15, 16 and 17. As discussed above, and in Lakes and Katz (1979), these moduli are equal, both in linearly viscoelastic solids and in those describable by nonlinear superposition. In a material described by a more general constitutive equation, such as presented in Lakes and Katz (1979), R and G can differ. For bovine bone, recovery follows relaxation $[R(t) = G(t)]$; however,

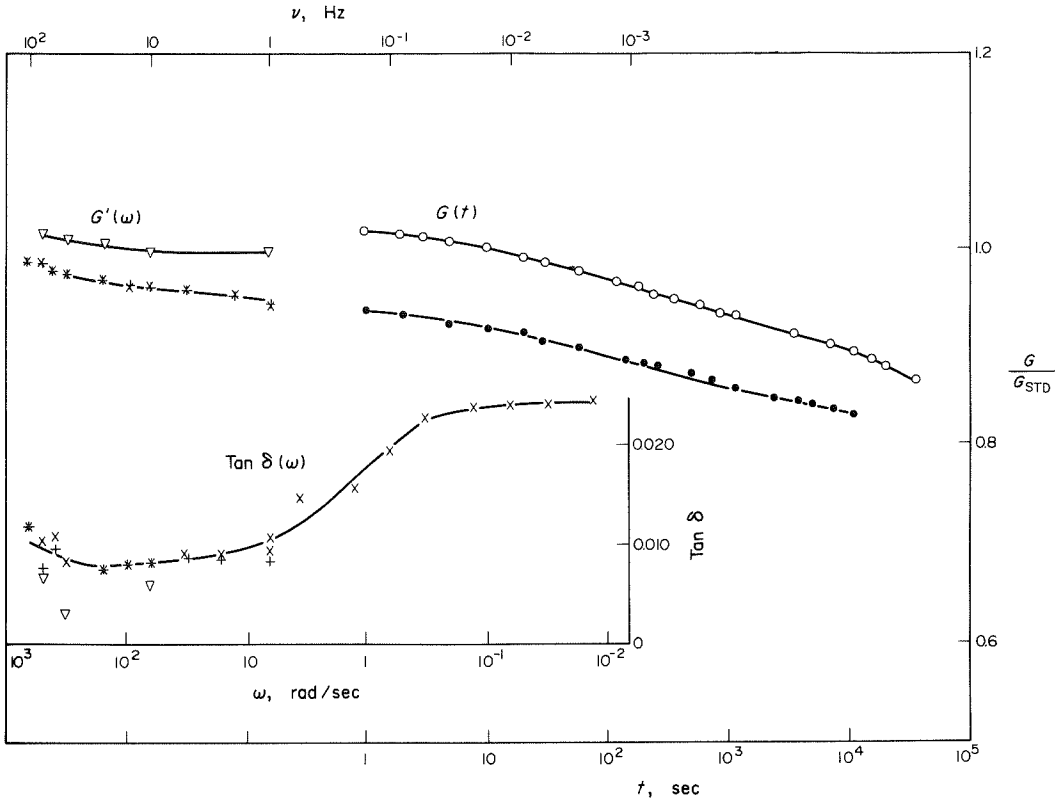

Fig. 14. Viscoelastic response in bovine femoral bone, specimen 9; $T = 36.7°C$.

● Relaxation $\gamma = 1.71 \times 10^{-4}$
○ Relaxation $\gamma = 7.89 \times 10^{-4}$
\+ Dynamic $\gamma = 1.71 \times 10^{-5}$
× Dynamic $\gamma = 1.71 \times 10^{-4}$
▽ Dynamic $\gamma = 7.89 \times 10^{-4}$

Simple torsion
$G_{STD} = 8.62 \times 10^5 lb/in^2$.

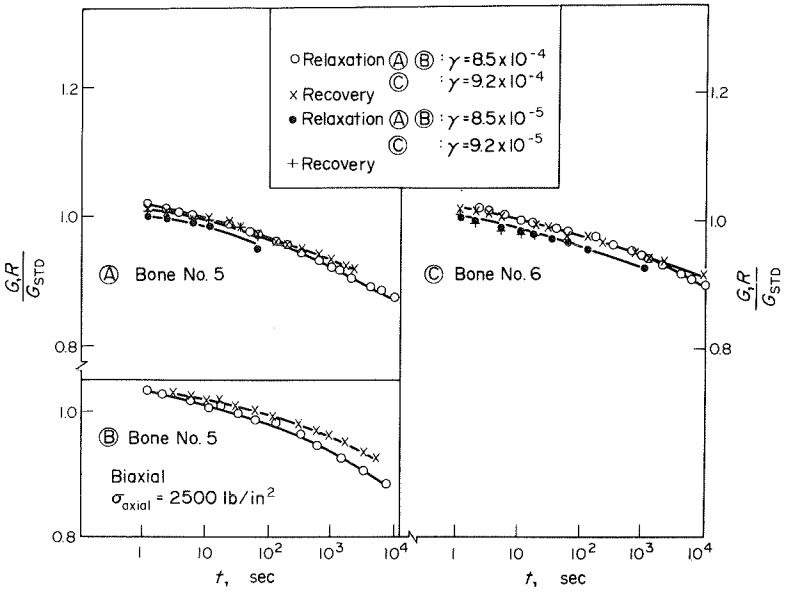

Fig. 15. Relaxation and recovery for two different specimens (numbers 5, 6) of wet human tibial bone; $T = 37°C$.

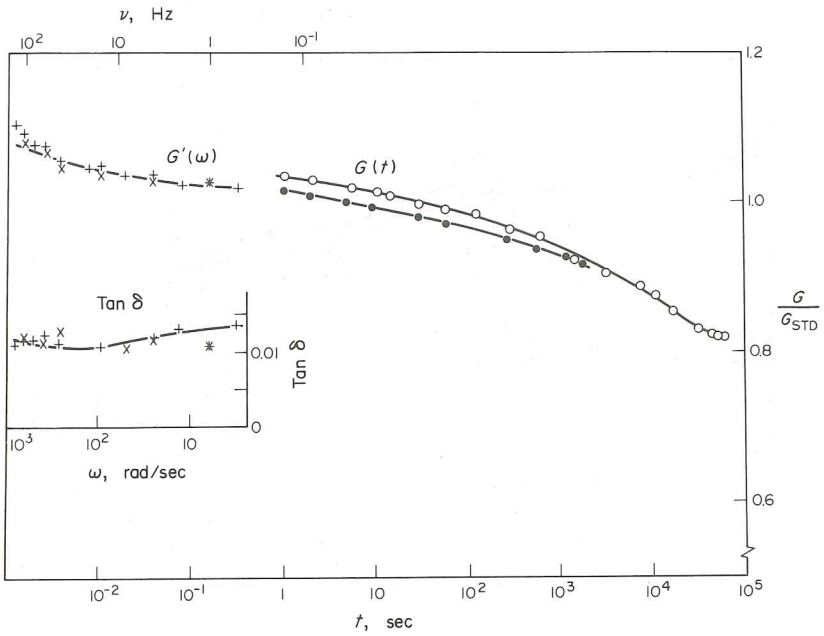

Fig. 19. Viscoelastic response in biaxial mode for wet human tibial bone, specimen 5; $T = 37°C$; $\sigma_{axial} = 2500$ lb/in^2. Symbols as for Fig. 18.

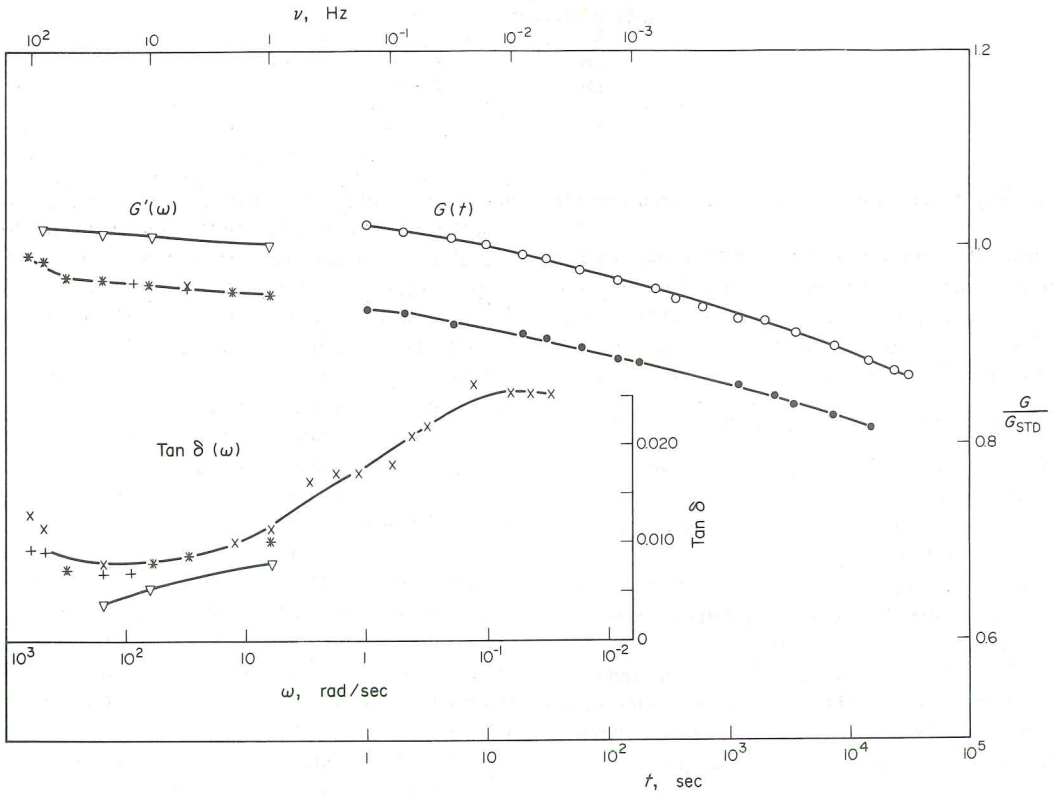

Fig. 20. Biaxial viscoelastic response of wet bovine femoral bone, specimen 9; $T = 36.7°C$.

● Relaxation $\gamma = 1.71 \times 10^{-4}$
○ Relaxation $\gamma = 7.89 \times 10^{-4}$
+ Dynamic $\gamma = 1.71 \times 10^{-5}$
× Dynamic $\gamma = 1.71 \times 10^{-4}$
▽ Dynamic $\gamma = 7.89 \times 10^{-4}$
Biaxial $\sigma_{axial} = 3200$ lb/in^2
$G_{STD} = 8.62 \times 10^5$ lb/in^2.

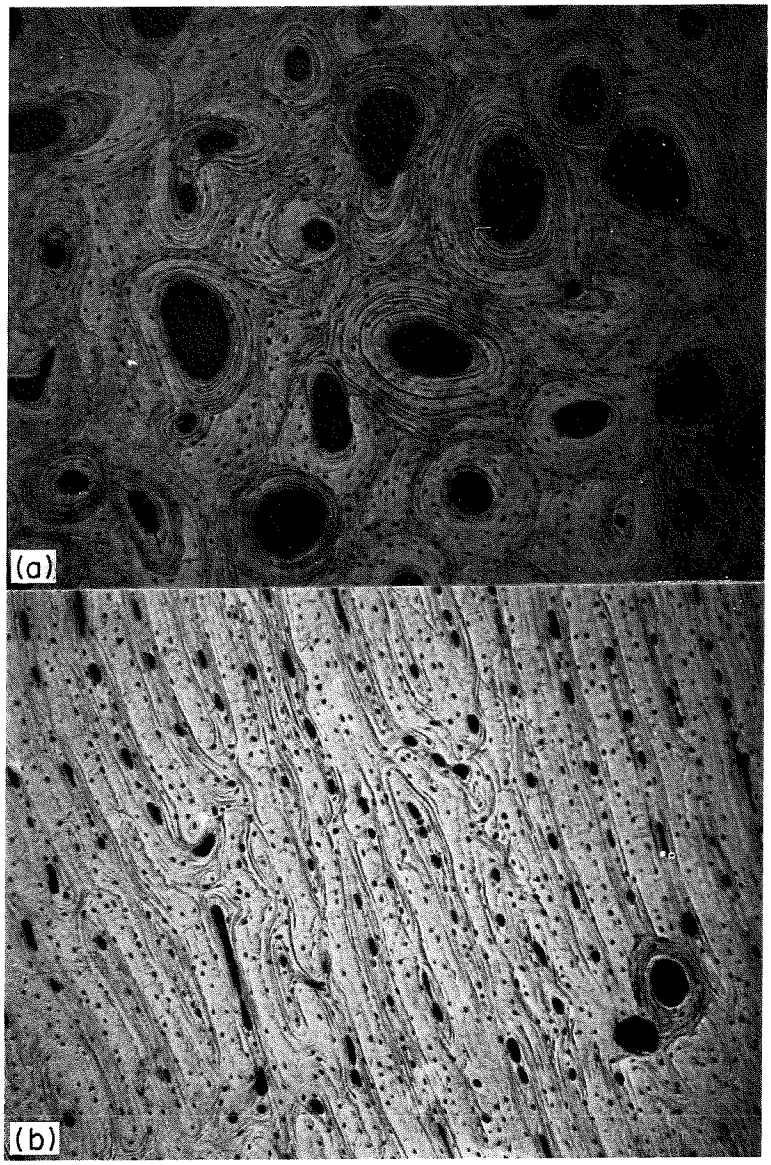

Fig. 21. A comparison of the microstructure of typical human haversian bone (a) and bovine plexiform bone (b) (after Yoon and Katz, 1976a). Femur, 67×. Cross section perpendicular to bone axis.

polystyrene–rubber composite in torsion is increased by as much as 30% in the presence of an axial tensile stress 6.38 MN/m^2. The shear modulus was decreased by about 4.2% in the frequency range 0.01–10 Hz by an axial stress 6.25 MN/m^2 and the β peak associated with the styrene phase was shifted to higher frequency. By contrast, maximum changes in the shear modulus for bone in the present work were 1.5% for human bone (σ_{axial} = 17.2 MN/m^2) and 0.63% for bovine bone (σ_{axial} = 22.1 MN/m^2).

Recovery following biaxial relaxation is shown in Figs. 15 and 17. For human bone, recovery occurs more slowly than relaxation at long times; this effect is accentuated by the presence of an axial load. For bovine bone, this nonlinearity in response is not resolvable in simple torsion at the strains used; however, it appeared in the presence of an axial load.

In summary, the present experiments have shown that bone exhibits viscoelastic behavior throughout the eight decade region of time-scale studied. This behavior is thermorheologically complex, non-linear and stress-field dependent. Individual bone specimens differ in both the time-dependence and the strain-dependence of G so that a unique kernel characteristic of 'bone' cannot be written. The thermorheological complexity of the bone suggests multiple mechanisms for the viscoelastic response. In order to understand this behavior, hypothetical relaxation mechanisms have been examined theoretically in the second paper of this series (Lakes and Katz, 1979a). Finally, the availability of the present viscoelastic data for behavior of bone over eight decades has allowed a serious attempt at deriving a constitutive equation to describe the nonlinear torsional response of bone. This description is developed in detail in the third paper of this series (Lakes and Katz, 1979b).

Acknowledgement – Contribution 86 from the Laboratory for Crystallographic Biophysics. This research was supported in part by the National Institutes of Health–National Institute of Dental Research, Training Grant 5T1-DE-117-13.

REFERENCES

Ascenzi, A. and Bonucci, E. (1966) The compressive properties of single osteons. *Anat. Rec.* **161,** 337–392.

Bird, F., Becker, H., Healer, J. and Messer, M. (1968) Experimental determination of the mechanical properties of bone. *Aero. Med.* **39,** 40–48.

Black, J. and Korostoff, E. (1973) Dynamic mechanical properties of viable human cortical bone. *J. Biomechanics* **6,** 435–438.

Bonfield, W. and Li, C. H. (1967) Anisotropy of nonelastic flow in bone. *J. appl. Phys.* **38,** 2450–2455.

Currey, J. D. (1965) Anelasticity in bone and echinoderm skeletons. *J. exp. biol.* **43,** 279–292.

Dempster, W. T. and Liddicoat, R. T. (1952) Compact bone as a non-isotropic material. *Am. J. Anat.* **91,** 331–362.

Evans, F. G. (1973) *Mechanical Properties of Bone.* Thomas, Springfield.

Ferry, J. D. (1970) *Viscoelastic Properties of Polymers.* Wiley, New York.

Frasca, P. (1974) Structure and dynamic mechanical properties of human single osteons. Ph.D. Thesis. Rensselaer Polytechnic Institute, Troy, New York.

Haelen, G. and Sternstein, S. S. (1977) Viscoelastic properties of bovine bone. Paper presented at the Society of Rheology Meeting, Oct. 23–27. Madison, Wisconsin.

Katz, J. L. and Mow, V. C. (1973) Mechanical and structural criteria for orthopaedic implants. *Biomat., Med. Dev. Art. Org.* **1,** 575–638.

Lakes, R. S. and Katz, J. L. (1974) Interrelationships among the viscoelastic functions for anisotropic solids: application to calcified tissues and related systems. *J. Biomechanics* **7,** 259–270.

Lakes, R. S. and Katz, J. L. (1979a) Viscoelastic properties of wet cortical bone—II. Relaxation mechanisms. *J. Biomechanics* **12,** 679–687.

Lakes, R. S. and Katz, J. L. (1979b) Viscoelastic properties of wet cortical bone—III. A constitutive equation. *J. Biomechanics* **12,** 689–698.

Lang, S. B. (1969) Elastic coefficients of animal bone. *Science, N.Y.* **165,** 287.

Lugassy, A. A. and Korostoff, E. (1969) Viscoelastic behavior of bovine femoral cortical bone and sperm whale dentin. *Research in Dental and Medical Materials.* Plenum Press, New York.

Myers, F. A., Cama, F. C. and Sternstein, S. S. (1976) Mechanically enhanced aging of glassy polymers. *Ann. N.Y. Acad. Sci.* **279,** 94–99.

Myers, F. A. and Sternstein, S. S. (1977) Mechanically enhanced aging of glassy polymers. Paper presented at the Society of Rheology Meeting, Oct. 23–27. Madison, Wisconsin.

Paterno, J. (1970) The toughening mechanism in rubber modified glassy polymers. Ph.D. Thesis. Rensselaer Polytechnic Institute, Troy, New York.

Rauber, A. A. (1876) *Elasticität und Festigkeit der Knochen. Anatomisch–physiologische Studie.* Engelmann, Leipzig.

Smith, J. W. and Walmsley, R. (1959) Factors affecting the elasticity of bone. *J. Anat.* **93,** 503–523.

Smith, R. and Keiper, D. (1965) Dynamic measurement of viscoelastic properties of bone. *Am. J. med. Elec.* **4,** 156–160.

Turner, S. (1973) Creep in glassy polymers. *The Physics of Glassy Polymers* (Edited by Howard, R. H.). Wiley, New York.

Wertheim, G. (1847) Mémoire sur l'elasticité et la cohésion des principaux tissus du corps humain. *Annals Chim. Phys.* **21,** 385–414.

Yoon, H. S. and Katz, J. L. (1976a) Ultrasonic wave propagation in human cortical bone. I. Theoretical considerations for hexagonal symmetry. *J. Biomechanics* **9,** 407–412.

Yoon, H. S. and Katz, J. L. (1976b) Ultrasonic wave propagation in human cortical bone. II. Measurements of elastic properties and microhardness. *J. Biomechanics* **9,** 457–464.

APPENDIX 1

Bactericidal and Fungicidal Additive

Thimerosal	0.005 g
Aquatonic	0.2 ml
Fungistop	0.2 ml
Ringer's solution	6.0 ml

The thimerosal was obtained by evaporation of 5 ml of tincture merthiolate (thimerosal, 1:1000). 'Aquatonic' is an aquarium disinfectant made by Permalife, Inc. and consists of acriflavine (neutral) 0.045%, methylene blue 0.0074, balance H_2O. 'Fungistop', made by TetraCare, Inc., is an aquarium fungicide containing colloidal silver, natrium chloratum, magn. sulphuric, H_2O 99.816%.

APPENDIX 2

Obtaining Phase Angles from Lissajous Figures

Let $x = B \sin t$, $y = C \sin(\omega t + \delta)$. This represents an elliptical Lissajous figure; let the point where it crosses the $+x$ axis be called $(x, y) = (A, 0)$ and a time when this occurs be called t_1. Then $A = B \sin \omega t_1$, $0 = C \sin(\omega t_1 + \delta) = C \sin \omega t_1 \cos \delta + C \cos \omega t_1 \sin \delta$. But $\sin \omega t_1 = A/B$ substituted in the last expression, with $\cos \omega t_1 = \sqrt{B^2 - A^2}/B$ yields $0 = C(A/B)\cos \delta = (C\sqrt{B^2 - A^2}/B)\sin \delta$, or $A \cos \delta = \sqrt{B^2 - A^2} \sin \delta$. Squaring the last expression, $A^2 \cos^2 \delta = B^2 \sin^2 \delta - A^2 \sin^2 \delta$, which gives $A^2(\sin^2 \delta + \cos^2 \delta) = B^2 \sin^2 \delta$, so that $\sin \delta = A/B$.